CHIN. PHYS. LETT. Vol. 35, No. 11 (2018) 119401

Effect of Kinetic Alfvén Waves on Electron Transport in an Ion-Scale Flux Rope *

Bin-Bin Tang(唐斌斌)[1**], Wen-Ya Li(李文亚)[1], Chi Wang(王赤)[1], Lei Dai(戴磊)[1], Jin-Peng Han(韩金鹏)[2]

[1]*State Key Laboratory of Space Weather, National Space Science Center, Chinese Academy of Sciences, Beijing 100190*
[2]*Research and Development Center, China Academy of Launch Vehicle Technology, Beijing 100076*

(Received 6 August 2018)

At the Earth's magnetopause, the electron transport due to kinetic Alfvén waves (KAWs) is investigated in an ion-scale flux rope by the Magnetospheric Multiscale mission. Clear electron dropout around 90° pitch angle is observed throughout the flux rope, where intense KAWs are identified. The KAWs can effectively trap electrons by the wave parallel electric field and the magnetic mirror force, allowing electrons to undergo Landau resonance and be transported into more field-aligned directions. The pitch angle range for the trapped electrons is estimated from the wave analysis, which is in good agreement with direct pitch angle measurements of the electron distributions. The newly formed beam-like electron distribution is unstable and excites whistler waves, as revealed in the observations. We suggest that KAWs could be responsible for the plasma depletion inside a flux rope by this transport process, and thus be responsible for the formation of a typical flux rope.

PACS: 94.05.Pt, 94.30.ch DOI: 10.1088/0256-307X/35/11/119401

Magnetic flux ropes are 3D helical magnetic structures, with a transient bipolar magnetic field signature in the cross section. These flux ropes, when formed at the Earth's magnetopause, provide a channel for the mass and energy transfer from the solar wind into geospace.[1−4] Typically, flux ropes are characterized by a magnetic field enhancement along the axial direction, but also there are some that are detected with a magnetic dip in the center, referred as the crater flux rope, in which the plasma is denser to maintain the force balance.[5,6] Statistically, crater flux ropes are much less frequently observed than typical flux ropes, though the external solar wind conditions are similar and no significant difference of the local time occurrence is found.[6] Considering that a flux rope is probably generated by multiple X-line reconnection in a current sheet,[7,8] Zhang *et al.*[6] proposed that a flux rope is initially formed as a crater type and evolves into a typical one with a reduction of central plasma pressure resulting from the plasma transport along the axis, as the parallel plasma speed inside a crater flux rope could be larger than that in a typical flux rope. Therefore, the rarity of crater flux ropes in the observation might imply that the evolution from a crater type to a typical type would be fast. The development of a crater type flux rope to a typical one has also been revealed by a recent magnetohydrodynamic simulation with the embedded particle-in-cell model.[9]

Various wave activities inside a flux rope have been observed, such as kinetic Alfvén waves (KAWs), lower hybrid drift waves, whistler waves and electrostatic solitary waves.[10,11] Among these waves, low-frequency KAWs, developed when the perpendicular wavenumber of ideal Alfvén waves ($k_\perp$) is close to ion gyroradius (ρ_i), have attracted research interest, as they can effectively generate parallel electric field and magnetic field fluctuations.[12,13] It has been demonstrated that energy can transfer between KAWs and plasma particles via the transit-time interactions, as the instantaneous $\Delta(\boldsymbol{j}\cdot\boldsymbol{E})$ is nonzero,[14] and/or via the Landau resonance with an efficient widening of the resonance region due to the wave parallel field and the magnetic mirror force.[15,16] Though KAWs have been widely reported in the solar wind, the magnetic reconnection region, the magnetospheric plasma sheet boundary layer and the auroral acceleration region,[14,17−22] the possible effects of KAWs on plasma particles transport inside a flux rope have not been carefully investigated.

In this Letter, we focus on how KAWs can affect the electron transport in an ion-scale flux rope using high-resolution data from the Magnetospheric Multiscale (MMS) mission:[23] we use plasma data from the fast plasma investigation (FPI),[24] magnetic field data from the fluxgate magnetometer (FGM)[25] and the search coil magnetometer (SCM),[26] and electric field data from the electric field double probes (EDP),[27,28] respectively. The flux rope investigated was observed on 28 November 2016 between 10:44:41.5 UT and 10:44:46.0 UT. In this time interval, the four MMS spacecrafts were located approximately at [10.6, 5.1, 0.2] R_E in geocentric solar ecliptic (GSE) coordinates (Fig. 1(k)), and the spacecraft were in a tetrahedron formation with a separation smaller than 10 km (Fig. 1(l)). Due to the small separation, data from the four spacecraft are similar, and we show data primarily from MMS 1.

*Supported by the National Natural Science Foundation of China under Grant Nos 41474145, 41574159, 41731070 and 41504114, the Frontier Science Foundation of the Chinese Academy of Sciences under Grant No QYZDJ-SSW-JSC028, the Strategic Priority Research Program of the Chinese Academy of Sciences under Grant No XDA15052500, and the Specialized Research Fund for State Key Laboratories of China.

**Corresponding author. Email: bbtang@spaceweather.ac.cn

© 2018 Chinese Physical Society and IOP Publishing Ltd

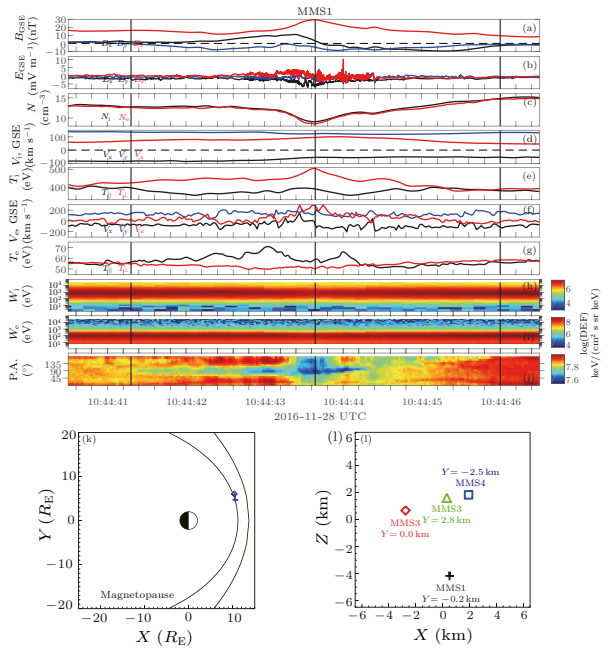

Fig. 1. Overview of the flux rope observed by MMS 1 on 28 November 2016: (a) $\boldsymbol{B}$, (b) $\boldsymbol{E}$, (c) $N_{\rm i}$ and $N_{\rm e}$, [(d), (e)] the ion bulk velocity and temperature, [(f), (g)] the electron bulk velocity and temperature, [(h), (i)] the ion and electron omnidirectional energy flux and (j) electron pitch angle distributions. Flux rope edges and magnetic maximum point are marked by the three vertical black lines. (k) Equatorial projection of the MMS orbit on 2016-11-28 from 10:00 to 12:00 UT, and the diamond marks the ending location of MMS and (l) spacecraft relative positions.

Overview of the flux rope, which is observed about ten seconds after the magnetopause crossing (not shown), is presented in Fig. 1. The flux rope is characterized by (i) a large bipolar variation of $B_{\rm X}$, changing from $\sim$10 nT to ~ -10 nT (Fig. 1(a)); (ii) a strong magnetic core near the $B_{\rm X}$ reversal, reaching $\sim$30 nT (Fig. 1(a)); (iii) a density dip simultaneously (Fig. 1(c)); and (iv) a flow enhancement of V_Z (Fig. 1(d)). From four-spacecraft timing analysis on the magnetic field, we estimate the flux rope speed to be $\sim$155 km/s along the direction $[-0.13, 0.92, 0.44]$ in GSE, suggesting a size of $\sim$770 km, or 11.3 ion inertial lengths ($d_{\rm i}$) considering an average ion number density of $\sim$11.2 cm^{-3}. The particle temperature exhibits significant anisotropy: for ions, it is $T_{\perp} > T_{||}$ (Fig. 1(e)), and for electrons, it is $T_{||} > T_{\perp}$ (Fig. 1(g)). The most outstanding phenomena in this case are the electron pitch angle distributions (Fig. 1(j)), which show that the electron energy flux around 90° is smaller inside the flux rope, and this decrease lasts except that the plasma density is significantly depleted in the magnetic reversal region.

Fluctuations around $\sim$1 Hz from plasma and field measurements are detected inside the flux rope (Fig. 2). Plasma and magnetic field data are high-pass filtered for frequencies larger than 0.9 Hz, and a band-pass filter between 0.9 Hz and 2 Hz is applied for the electric field to remove high frequency fluctuations. The maximum amplitude of these monochromatic fluctuations are $\Delta N_{\rm e}/N_{\rm e} \sim 0.07$ and $\Delta B/|B| \sim 0.1$. Compressive fluctuations are observed in anti-correlated electron density ($\Delta N_{\rm e}$) and magnetic field magnitude ($\Delta|B|$) (Figs. 2(a) and 2(b)). The amplitude of $\Delta B_{||}$ is almost equal to $\Delta B_{\perp}$, and is 90° out of phase (Fig. 2(c)). From electric field and magnetic field power spectrograms (Figs. 2(e) and 2(f)), the fluctuations are significant between 10:44:41.6 UT and 10:44:45.5 UT, just inside the flux rope and peaked in the central flux rope region. Wave ellipticity and wave angle are presented based on the singular value decomposition (SVD) method,[29] which shows that the wave is right-hand polarized (Fig. 2(g)), and the wave vector is directed almost perpendicular to the local magnetic field (Fig. 2(h)). All these signatures are consistent with compressive kinetic Alfvén waves.[12,30] The ion temperature anisotropy can be explained by the coupling between KAWs and ions, which can result into stochastic ion energization perpendicular to the magnetic field.[31] The parallel electric field embedded in KAWs can energize electrons in the parallel direction,[21,32] and we will investigate this process in detail in the following. During wave interval, the average background magnetic field, the plasma density and the corresponding Alfvén speed ($V_{\rm A}$) is about $20\times[0.17, -0.28, 0.95]$ nT, 11.2 cm^{-3} and 130 km/s.

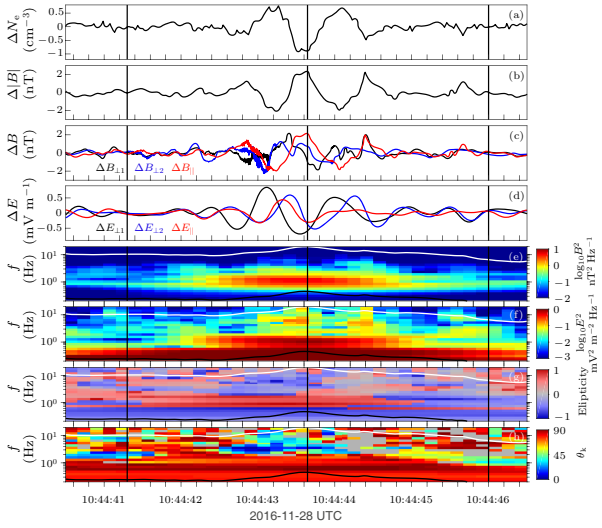

Fig. 2. MMS 1 observations of KAWs: (a) $\Delta N_{\rm e}$, (b) $\Delta|B|$, (c) $\Delta\boldsymbol{B}$, (d) $\Delta\boldsymbol{E}$ in the field-aligned coordinates, (e) magnetic field power spectrogram, (f) electric field power spectrogram, (g) wave ellipticity, and (h) wave angle. Plasma and magnetic field are high-pass filtered for $f > 0.9$ Hz, while a band-pass filter between 0.9 Hz and 2 Hz is applied for the electric field. The white and black curves in the bottom four panels are local lower hybrid frequency ($f_{\rm LH}$) and proton gyro frequency ($f_{\rm cp}$), while three vertical black lines mark the flux rope edges and magnetic maximum point.

Different methods are applied to estimate the KAW phase speed in the parallel direction ($\omega/k_{||}$). First, we calculate the ratio of the fluctuated electric field and magnetic field in the perpendicular direction, showing $\omega/k_{||} = \Delta E_{\perp}/\Delta B_{\perp} \approx 3.71 V_{\rm A}$. In the second method, since the spacecraft separation is much smaller than the ion gyro-radius, the multi-spacecraft

timing method is valid to determine the wave vector on the filtered magnetic field. It shows $\boldsymbol{k} = 0.035 \times [0.20, -0.89, -0.41]\,\mathrm{km}^{-1}$, corresponding to a wave angle (θ_{kB}) ~96° with respect to the background magnetic field and $k_\perp \rho_\mathrm{i} \approx 3.69$. This indicates that the wave is propagated anti-parallel to the background magnetic field. With the help of the KAW dispersion relation written as $\omega/k_{||} = V_\mathrm{A}\sqrt{1 + k_\perp^2 \rho_\mathrm{i}^2 (1 + T_\mathrm{e}/T_\mathrm{i})}$, we can infer that $\omega/k_{||} \approx 4.05 V_\mathrm{A}$. In the third method, considering electrons remain magnetized throughout the wave packet, electron transverse velocity fluctuations should satisfy $\Delta \boldsymbol{v}_{\mathrm{e},\perp} = -(\omega/k_{||}) \times (\Delta \boldsymbol{B}_\perp / B)$.[14] Therefore, the parallel speed can be directly evaluated by fitting $\Delta \boldsymbol{v}_{\mathrm{e},\perp}/V_\mathrm{A}$ and $\Delta \boldsymbol{B}_\perp / B$. The result (see the supplementary material) shows that $\omega/k_{||} \approx 4.23 V_\mathrm{A}$ with a correlation coefficient of 0.89. The positive correlation indicates again that the wave propagates anti-parallel to the local magnetic field. Thus, the wave parallel speed from these different methods is in good agreement with each other, suggesting an average value of $3.99 \pm 0.26 V_\mathrm{A}$.

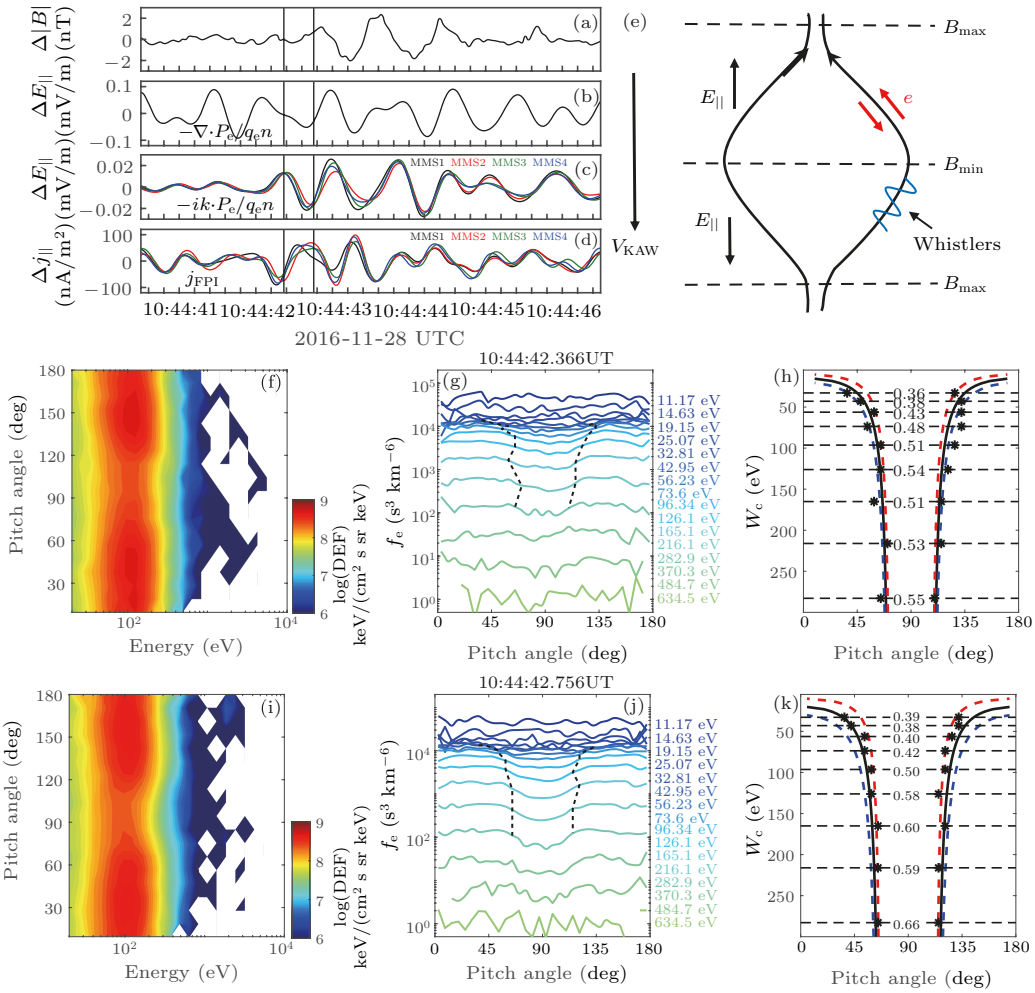

Fig. 3. Properties of KAWs and associated electron trapping: (a) $\Delta|\boldsymbol{B}|$, (b) $\Delta \boldsymbol{E}_{||}$ from $-\nabla \cdot \boldsymbol{P}_\mathrm{e}/(n_\mathrm{e} q_\mathrm{e})$, (c) $\Delta \boldsymbol{E}_{||}$ from $-i\boldsymbol{k} \cdot \boldsymbol{P}_\mathrm{e}/(n_\mathrm{e} q_\mathrm{e})$, and (d) $\Delta \boldsymbol{j}_{||}$ from direct plasma measurements. A band-pass filter (0.9 Hz< f <2 Hz) is used for the electric field and current density. Electron measurements marked by two black vertical lines are presented in the following panels. (e) A cartoon of electron trapping by KAWs. Electron distributions at 10:44:42.366 UT: (f) pitch angle-energy distributions, (g) phase space density as a function of energy and pitch angle, and (h) comparison of electron dropout from observation and theoretical analysis (Eq. (1)). The red, black and blue curves are estimated from $\Phi_0 = 10$, 15 and 20 V with $B_\mathrm{min}/B_\mathrm{max} = 0.92$ and the numbers represent the normalized electron dropout at each energy channel, defined by $(f_\mathrm{max} - f_\mathrm{min})/f_\mathrm{max}$. (i)–(k) Similar to (f)–(h), but at 10:44:42.756 UT, while the parameters used in (k) are $\Phi_0 = 10$, 20 and 30 V and $B_\mathrm{min}/B_\mathrm{max} = 0.85$.

The estimated KAW parallel speed is generally much less than the electron parallel velocity ($v_{||}$), whose thermal velocity can usually be several thousands of km/s or even larger. Therefore, the Landau resonance condition ($k_{||} v_{||} = \omega$) is not easily satisfied. However, the resonance region can be efficiently widened due to the presence of the wave parallel field and the mirror force, which allows electrons to be able to move with the parallel phase speed of the wave. This means that the resonance would be favorable at $v_{||} \in [\omega/k_{||} \pm \sqrt{e\Delta W/m_\mathrm{e}}]$, where ΔW is the variation of electron parallel energy.[15,33] Since the wave parallel speed is relatively small, an approximate condition for electron resonance is that electrons are ini-

tially trapped by KAWs. Theoretically, inside a wave packet, an electron is trapped when its pitch angle (θ) at the magnetic minimum should satisfy

$$\sin^2\theta \geq \frac{B_{\min}}{B_{\max}}(1 - e\Phi_0/W_c), \quad (1)$$

where Φ_0 is the wave potential, and W_c is the electron energy at $B_{\min}$. Therefore, (1) if $W_c < e\Phi_0$, electrons will be absolutely trapped; (2) if $W_c \gg e\Phi_0$, the pitch angle for trapped electrons will be roughly determined by $B_{\min}/B_{\max}$, which is consistent with magnetic mirrors.

The magnetic variation of KAWs is presented in Fig. 3(a). The wave potential, expressed as $\Phi_0 \sim E_{||}/k_{||}$, can be estimated from $E_{||}$. To avoid the uncertainties of both particle and field measurements,[14] this parallel electric field is inferred directly from the electron pressure gradient (that is, $-\nabla \cdot \boldsymbol{P}_e/(n_e q_e)$) and estimated from its plane-wave approximated value (that is, $-i\boldsymbol{k} \cdot \boldsymbol{P}_e/(n_e q_e)$) with a known wave vector ($\boldsymbol{k}$). The estimated electric field of these two methods, filtered by 0.9 Hz $< f <$ 2 Hz, is shown in Figs. 3(b) and 3(c). Both electric fields are roughly 90° out of phase with the magnetic field perturbations as expected, but their magnitude is different. This could be attributed to the accuracy of the wave vector directions and/or the goodness of the plane-wave approximation, but in general, the maximum wave potential is estimated to be ∼10–30 V.

A cartoon is presented in Fig. 3(e) to show variations of the magnetic field and parallel electric field in a KAW wave packet. Electrons that are trapped by the wave potential and the magnetic mirror force can then undergo Landau resonance with waves. The observed electron pitch angle distributions of energy flux at 10:44:42.366 UT clearly indicate that the electron differential energy flux with energy from tens of eV to several hundreds of eV presents a local minimum around 90° pitch angle (Fig. 3(f)). The measured electron phase space density (PSD) shows a similar decrease around 90° pitch angle (Fig. 3(g)). By finding the maximum gradient of PSD at each energy channel, we can evaluate the pitch angle range of the reduced electron PSD, and mark them with two dashed lines in Fig. 3(g). Then a comparison between this pitch angle range and the pitch angles for the trapped electrons in Eq. (1) is shown in Fig. 3(h). According to the local conditions ($B_{\min}/B_{\max} = 0.92$ and the wave potential is estimated from 10 V, 15 V to 20 V), three curves (red, black and blue) are plotted to show pitch angle range for trapped electrons, and it is in good agreement with the pitch angles of reduced electron PSD presented by the black dots. This further confirms that it is the trapped electrons that are transported away, and the most likely mechanism is the Landau resonance. After resonance, electrons are accelerated along the magnetic field lines, which results in an energy increase and associated pitch angle change. The normalized electron 'dropout' at each energy channel, defined by $(f_{\max} - f_{\min})/f_{\max}$, is then evaluated (Fig. 3(h)). The estimated maximum dropout is larger than 50% and electrons with energy as high as 200 eV can be affected.

A similar process is performed at 10:44:42.756 UT, when the waves are more intensive ($B_{\min}/B_{\max} = 0.85$, and Φ_0 is adopted from 10 to 30 V). The electron dropout around 90° is also revealed (Figs. 3(i)–3(k)). An interesting point is that the relative dropout is smaller for electrons from ∼50 to 100 eV at 10:44:42.756 UT compared with that at 10:44:42.366 UT, though the wave potential and magnetic mirror force are in general larger. This is due to a more widened resonance region from KAWs, through which electrons can gain more energy.[15]

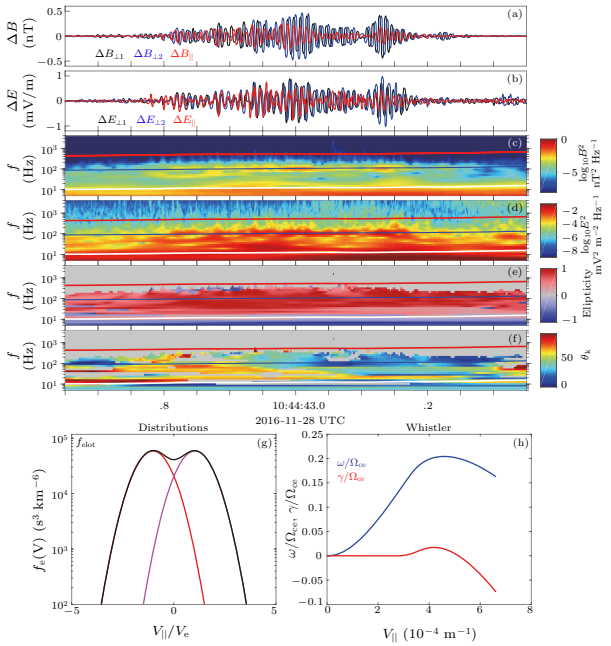

Fig. 4. Properties of whistler mode: (a) $\Delta\boldsymbol{B}$, (b) $\Delta\boldsymbol{E}$, (c) magnetic field power spectrogram, (d) electric field power spectrogram, (e) wave ellipticity, (f) wave angle, (g) two modeled electron distributions along the magnetic direction (red and magenta) and the sum (black) and (h) the associated whistler modes predicted from WHAMP code (blue for real frequency and red for growth rate). The field parameters in (a) and (b) are filtered between 80 Hz and 300 Hz. The red, blue and white curves in (c)–(f) are local electron gyro-frequency (f_{ce}), $0.2f_{ce}$ and local lower hybrid frequency (f_{LH}).

Meanwhile, the beam-like distributions with substantial sources of free energy can excite whistler waves.[34] Figure 4 shows MMS observations of the whistle waves. Significant perturbations of magnetic and electric fields are observed from both perpendicular and parallel directions, and its wave frequency is about $0.2f_{ce}$, as indicated by the blue curve in Figs. 4(c) and 4(d), where f_{ce} is the local electron gyro-frequency. The waves are right-hand polarized and oblique propagated. The wave parallel speed estimated by $\Delta\boldsymbol{E}$ and $\Delta\boldsymbol{B}$ is about 1300–1800 km/s. To further confirm if these whistler waves are generated by the beam-like electron distribution, we use

the dispersion equation solver WHAMP[35] to find the solutions from full linear kinetic theory. We assume two identical Maxwellian-distributed electron populations with different parallel speeds, and present them in Fig. 4(g). The partial moments of each population are roughly estimated from electrons with pitch angles larger and smaller than 90°, which are $N_e = 6\,\mathrm{cm}^{-3}$, $V_{e,||} = \pm 2500\,\mathrm{km/s}$, $T_{e,||} = 20\,\mathrm{eV}$ and $T_{e,\perp} = 50\,\mathrm{eV}$. The dispersion relation has a real frequency of about $0.2 f_{ce}$ when meeting the maximum growth rate (Fig. 4(h)), consistent with the observation of whistlers. The parallel speed is about 1500 km/s, which is smaller than electron parallel speed ($V_{e,||}$) as expected, and also in good agreement with observations. This indicates that the observed whistlers are generated by the beam-like distributions. These high-frequency whistlers can consequently interact with electrons, such as pitch-angle scattering[36] and energization,[37] suggesting a natural energy cascading process from ion scales corresponding to KAWs to smaller electron scales.

The efficiency of electron transport by KAWs should be further addressed. O'Neil[38] indicated that the nonlinear effect will prevent the complete wave damping on large time scales and the wave is sustained by the oscillations of the particles trapped in the wave's potential well. This nonlinear wave modulation is satisfied if the wave linear growth rate (γ_L) is far less than the particle bounce frequency (ω_b). Gershman *et al.*[14] demonstrated the conservative energy exchange between the particles and fields that comprise a nearly undamped KAW ($|\gamma_L/\omega| < 0.01$). From gyro-kinetic theory (Eq. (63)),[39] the linear growth rate of KAWs (γ_L/ω) functioned by $k_\perp \rho_i$ is estimated to be -0.024 for a large $k_\perp \rho_i$ ($\sim$3.69), allowing the wave amplitude to be half reduced in 4 to 5 wave periods. However, this damping rate may still not be strong enough compared with the electron bounce frequency, which is of the order of $\sim$1 Hz. On the other hand, KAWs here are detected inside a flux rope, where the background magnetic field is nonuniform. Thus the resonant interactions between electrons and waves are significantly modified by this magnetic field inhomogeneity, as the criteria $k_{||} R \gg 1$ is roughly satisfied, where R is the curvature radius of the magnetic field lines, varying from $\sim$500 to 2000 km.[40] This probably leads the trapped electrons to be accelerated and become more field-aligned.

Though we have shown MMS observations that the KAWs reported here can effectively transport electrons from the equatorial pitch angle to smaller pitch angles, KAWs alone are not able to cause the observed density depletion in the central flux rope, for their pitch angles could be still far from loss cone. Other succeeding local or remote processes, i.e., the interactions of electrons with the higher frequency waves discussed above, should further transport these electrons to even smaller pitch angles. Therefore, the density depletion inside a flux rope, or the evolution of a flux rope to a typical type should be a consequence of combined different processes, and the role of KAWs is to catalyze the electron depletions by transporting them into the field-aligned direction. This may explain why electron dropout at $\sim$90° pitch angle is found throughout the flux rope, but clear electron depletion is observed merely in the central flux rope region.

To summarize, we have presented MMS observations to show how KAWs can transport electrons in an ion-scale flux rope. The wave potential and the magnetic compressibility are two key factors to trap and then accelerate electrons to form unstable beam-like distributions. We propose that KAWs are responsible for the plasma loss inside the flux rope, which would benefit the quick evolution of a crater flux rope to a typical flux rope. Therefore, such wave-particle interactions are crucial to understand how flux ropes transport mass and energy from solar wind into geospace.

We thank the entire MMS team for providing high-quality data. MMS data are available at https://lasp.colorado.edu/mms/sdc/public/.

References

[1] Russell C T and Elphic R C 1978 *Space Sci. Rev.* **22** 681
[2] Paschmann G et al 1982 *J. Geophys. Res.* **87** 2159
[3] Hasegawa H et al 2010 *Geophys. Res. Lett.* **37** L16101
[4] Pu Z Y et al 2013 *Geophys. Res. Lett.* **40** 3502
[5] Farrugia C J et al 1988 *J. Geophys. Res.* **93** 14465
[6] Zhang H et al 2010 *J. Geophys. Res.* **115** A08229
[7] Lee L C and Fu Z F 1985 *Geophys. Res. Lett.* **12** 105
[8] Raeder J 2006 *Ann. Geophys.* **24** 381
[9] Chen Y et al 2017 *J. Geophys. Res.: Space Phys.* **122** 10318
[10] Øieroset M et al 2014 *J. Geophys. Res.* **119** 6256
[11] Huang S Y et al 2016 *Geophys. Res. Lett.* **43** 7850
[12] Holleweg J V 1999 *J. Geophys. Res.* **104** 14811
[13] Stasiewicz K et al 2000 *Space Sci. Rev.* **92** 423
[14] Gershman D J et al 2017 *Nat. Commun.* **8** 14719
[15] Artemyev A V et al 2015 *J. Geophys. Res.: Space Phys.* **120** 10305
[16] Damiano P A et al 2015 *J. Geophys. Res.: Space Phys.* **120** 5623
[17] Sahraoui F et al 2009 *Phys. Rev. Lett.* **102** 231102
[18] Dai L 2009 *Phys. Rev. Lett.* **102** 245003
[19] Dai L et al 2017 *Geophys. Res. Lett.* **44** 634
[20] Dai L 2018 *J. Geophys. Res.: Space Phys.* **123** (accepted)
[21] Wygant J R et al 2002 *J. Geophys. Res.* **107** (A8) 1201
[22] Chaston C C et al 2008 *Phys. Rev. Lett.* **100** 175003
[23] Burch J L et al 2016 *Science* **352** aaf2939
[24] Pollock C et al 2016 *Space Sci. Rev.* **199** 331
[25] Russell C T et al 2016 *Space Sci. Rev.* **199** 189
[26] Le Contel O et al 2016 *Space Sci. Rev.* **199** 257
[27] Lindqvist P A et al 2016 *Space Sci. Rev.* **199** 137
[28] Ergun R E et al 2016 *Space Sci. Rev.* **199** 167
[29] Santolik O et al 2003 *Radio Sci.* **38** 1
[30] Hunana P et al 2013 *Astrophys. J.* **766** 93
[31] Johnson J R and Cheng C Z 2001 *Geophys. Res. Lett.* **28** 4421
[32] Hasegawa A and Chen L 1976 *Phys. Rev. Lett.* **36** 1362
[33] Karney C F F 1978 *Phys. Fluids* **21** 1584
[34] Mourenas D et al 2015 *J. Geophys. Res.* **120** 3665
[35] Rönnmark K 1982 *WHAMP—Waves in Homogeneous, Anisotropic Multicomponent Plasmas* (Reports No. 179) (Kiruna, Sweden: Kiruna Geophysical Institute)
[36] Thorne R M et al 2010 *Nature* **467** 943
[37] Mourenas D et al 2012 *J. Geophys. Res.* **117** A10212
[38] O'Neil T 1965 *Phys. Fluids* **8** 2255
[39] Howes G G et al 2006 *Astrophys. J.* **651** 590
[40] Artemyev A V et al 2017 *J. Geophys. Res.: Space Phys.* **122** 5519

Supplemental Material: The effect of kinetic Alfvén waves on electron transport in an ion-scale flux rope

Bin-Bin Tang(唐斌斌),[1,*] Wen-Ya Li(李文亚),[1] Chi Wang(王赤),[1] Lei Dai(戴磊),[1] and Jin-Peng Han(韩金鹏)[2]

[1] *State Key Laboratory of Space Weather, National Space Science Center, Chinese Academy of Sciences, Beijing, 100190, China.*

[2] *Research and Development Center, China Academy of Launch Vehicle Technology, Beijing, 100076, China.*

To estimate the parallel phase speed ($\omega/k_{||}$) of kinetic Alfvén waves (KAWs), we consider the electron transverse velocity fluctuations throughout the KAW periods, which should satisfy $\Delta \boldsymbol{v}_{e,\perp} = -(\omega/k_{||}) \times (\Delta \boldsymbol{B}_\perp/B)$.[1] Figure 1 presents the correlation of $\Delta \boldsymbol{v}_{e,\perp}/V_A$ vs $\Delta \boldsymbol{B}_\perp/B$, where V_A is the Alfvén speed. The positive correlation coefficient (CC = 0.89) indicates that the wave propagates anti-parallel to the local magnetic field ($k_{||} < 0$). The slope of the linear fit of the fluctuations suggests the KAW parallel phase speed is about $4.23V_A$.

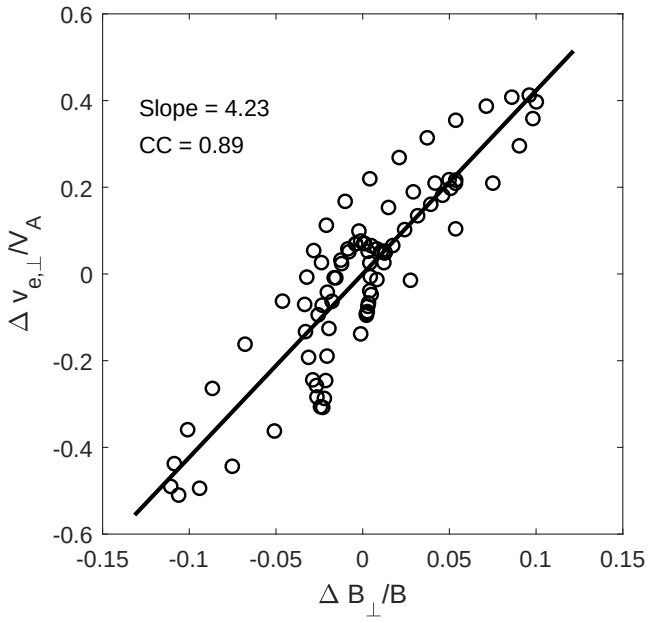

FIG. 1: Correlation of electron velocity and magnetic field fluctuations.

[1] Gershman D J et al. 2017 Nature Commun. **8** 14719

*Electronic address: bbtang@spaceweather.ac.cn